ACCSCIENCE PUBLISHING

Cancer Plus

ORIGINAL RESEARCH ARTICLE

Deciphering the prognostic significance of liquid–liquid phase separation-related genes in thyroid carcinoma: A transcriptomic analysis

Wenjun Zhao[1†], Peng Ma[1†], Yuesheng Wu[2], Kai Ma[1], Lei Zhang[1], Jian Wang[1], and Jun Zhao[1*]

[1]Department of Thyroid Surgery and Bariatric Metabolic Surgery, Shanxi Bethune Hospital, Taiyuan, Shanxi, China

[2]Department of Blood Transfusion, Shanxi Bethune Hospital, Taiyuan, Shanxi, China

Abstract

Thyroid carcinoma (THCA) is a common endocrine malignancy with heterogeneous clinical outcomes, and the prognostic significance of liquid–liquid phase separation (LLPS)-related genes in THCA remains unexplored. This study focuses on THCA, aiming to explore LLPS-related prognostic genes to provide novel theoretical foundations for its diagnosis and treatment. Utilizing public datasets, we identified LLPS-associated prognostic genes in THCA via differential expression analysis, Cox regression, and machine learning. A risk prediction model was subsequently constructed, followed by drug-sensitivity analysis, while the expression of prognostic genes was validated using reverse transcription-quantitative polymerase chain reaction (RT-qPCR). The results revealed seven key prognostic genes: *APOE*, *ARHGEF4*, *CCL17*, *DYRK3*, *EGF*, *HSPA1A*, and *MAP1B*. The risk model demonstrated strong predictive performance, with area under the curve values exceeding 0.7 for survival rate prediction. Cox regression analysis indicated that both the risk score and age were significant prognostic factors, with the risk score exhibiting a stronger independent prognostic effect (hazard ratio = 2.328). The nomogram accurately predicted survival, and drug-sensitivity analysis showed significant differences in responses to paclitaxel and cyclophosphamide between different risk groups. RT-qPCR validation confirmed upregulation of *APOE*, *CCL17*, *ARHGEF4*, *DYRK3*, *HSPA1A*, and *MAP1B*, along with downregulation of *EGF* in the THCA group. In conclusion, the identified prognostic genes and risk score model hold potential clinical value in predicting THCA outcomes, contributing to the development of personalized treatment strategies.

Keywords: Thyroid carcinoma; Liquid–liquid phase separation; Transcriptomics; Nomogram; Risk score; Prognosis

†*These authors contributed equally to this work.*

***Corresponding author:**
Jun Zhao
(zhaojun@sxbqeh.com.cn)

Citation: Zhao W, Ma P, Wu Y, *et al*. Deciphering the prognostic significance of liquid–liquid phase separation-related genes in thyroid carcinoma: A transcriptomic analysis. *Cancer Plus*. doi: 10.36922/CP025320050

Received: August 8, 2025

Revised: June 11, 2026

Accepted: June 26, 2026

Published online: July 20, 2026

1. Introduction

Thyroid carcinoma (THCA) represents a prevalent endocrine malignancy exhibiting a dramatically escalating global incidence in recent decades.[1] While generally associated with favorable mortality rates, THCA demonstrates remarkably high recurrence/persistence rates.[2] Current management is risk-adapted, ranging from active surveillance/minimally invasive approaches for low-risk disease to systemic therapies for advanced

cases.[3] However, aggressive variants and radioiodine-refractory THCA remain therapeutically challenging, as available systemic treatments often provide limited survival benefit with considerable toxicity.[4,5] Therefore, identifying robust prognostic biomarkers and developing reliable risk stratification tools are of clear clinical importance. In addition to tumor-intrinsic alterations, increasing evidence suggests that the tumor immune microenvironment and immune-cell infiltration contribute to THCA progression, immune escape, and therapeutic response[6–8], highlighting the value of integrating prognostic signatures with immune-related features.

Liquid–liquid phase separation (LLPS) is an intrinsic biophysical process that organizes proteins and RNAs into dynamic membraneless condensates, thereby regulating diverse cellular functions.[9–11] Accumulating evidence indicates that LLPS is closely involved in oncogenesis and cancer progression.[9,12,13] For instance, the transcriptional coactivators Yes-associated protein/transcriptional coactivator with PDZ-binding motif orchestrate oncogenic transcriptional programs through LLPS-mediated compartmentalization, while chromosomal translocations that generate pathological fusion proteins may disrupt normal LLPS dynamics, thereby driving malignant transformation.[14] Clinically, aberrant LLPS has been implicated in the pathogenesis of various malignancies, including esophageal cancer[15], breast cancer[16], prostate cancer[17], and gliomas.[18] However, the prognostic relevance of genes annotated as LLPS-related, as well as their potential associations with the immune microenvironment in THCA, remains insufficiently explored. Therefore, a systematic investigation of LLPS-related transcriptional features may help identify prognostic biomarkers and generate hypotheses regarding the possible involvement of LLPS-associated molecular programs in THCA.

In light of this research background, this study innovatively integrates The Cancer Genome Atlas (TCGA)-THCA public database data with clinical information to construct, for the first time, a risk prediction model based on the expression patterns of LLPS-related genes in THCA patients. After stratifying THCA patients using this model, we found significant differences across risk groups in prognosis, clinicopathological features, and the tumor immune microenvironment. Notably, this study, to our knowledge, is among the first to construct a prognostic model based on LLPS-related gene expression in THCA. This innovative model not only provides precise evidence for personalized prognostic assessment in THCA patients but also holds promise for informing clinical treatment decisions.

2. Materials and methods

2.1. Data source

University of California, Santa Cruz Xena database (https://xenabrowser.net/datapages/, accessed on October 18, 2024) was used to obtain the transcriptomic data for THCA. The TCGA-THCA dataset included corresponding clinical characteristics and follow-up information, encompassing age, gender, tumor stage, TNM stage, and overall survival (OS), with a total of 572 samples. According to the histopathological annotations in TCGA-THCA, the cohort is predominantly composed of papillary THCA (PTC) cases (≈99%), with only 4 non-PTC cases (Table S1). Therefore, the present analyses mainly reflect PTC biology. Only samples designated as 01A and 11A were retained, with "A" designation indicating high quality. Ultimately, a total of 557 samples were preserved for analysis, consisting of a control group comprising 57 samples and a cancer group of 500 samples. Among these, survival information was available for 499 samples. Subsequently, the tumor samples from TCGA-THCA were divided into training (70%) and validation (30%) sets in a ratio of 7:3. In addition, the Data Resource of LLPS (DrLLPS) (https://llps.biocuckoo.cn/) was used to retrieve 1,137 genes related to LLPS. After the removal of duplicate entries, a final count of 1,065 unique LLPS-related genes was established.

2.2. Differential expression analysis

The "DESeq2" package (v 1.40.2)[19] in R (v 4.2.2, R Foundation for Statistical Computing, Austria) was utilized to identify differentially expressed genes (DEGs) between tumor cohorts and control cohorts within the TCGA-THCA dataset. The filtering criteria were established as follows: $|\mathrm{Log_2FC}| > 0.5$ and $p.\mathrm{adjust} < 0.05$. The "ggplot2" (v 3.3.6)[20] and "pheatmap" (v 1.0.12)[21] packages were used to generate volcano plots and heatmaps to visualize differential gene expression. The "ggvenn" package (v 0.1.9)[22] was employed to conduct an intersection analysis between the DEGs and LLPS-related genes. This analysis identified differentially expressed LLPS-related genes, which were subsequently visualized.

2.3. Enrichment analysis of differentially expressed liquid–liquid phase separation-related genes and construction of protein–protein interaction network

The "clusterProfiler" package (v 4.7.1.001)[23] was used to further investigate the differentially expressed LLPS-related genes using Gene Ontology (GO) and Kyoto Encyclopedia of Genes and Genomes (KEGG) ($p < 0.05$). The top eight most significant entries from each GO category and the

top 15 significant KEGG pathways were visualized using the "enrichplot" package (v 1.12.2).[24] Protein–protein interactions (PPIs) among the differentially expressed LLPS-related genes were determined using the Search Tool for the Retrieval of Interacting Genes/Proteins database (https://string-db.org/), with a minimum confidence score of 0.4. Cytoscape (v 3.8.2, Institute for Systems Biology, USA)[25] was employed to visualize the resulting PPI network.

2.4. Construction and validation of the risk model

To identify genes associated with the survival of THCA, univariate Cox regression analysis was conducted on the differentially expressed LLPS-related genes using the "survival" package (v 3.5-3)[26] based on the training cohort. Subsequently, the "glmnet" package (v 4.1.4)[27] was employed to incorporate these genes into the least absolute shrinkage and selection operator (LASSO) algorithm, and the LASSO model with the lowest error was selected as the final analytical result. Ultimately, prognostic genes associated with THCA were identified.

In the training cohort, the risk score for THCA patients was determined based on the expression levels and regression coefficients of each prognostic gene. Subsequently, the median risk score was used to classify patients into high-risk groups (HRGs) and low-risk groups (LRGs). The risk score formula was $risk\ score = \sum_{i=1}^{n}(coefi * Xi)$, where *Xi* was the relative expression of prognostic genes, and *coefi* was the coefficient of each prognostic gene. Furthermore, the "timeROC" package (v 1.0.3)[28] was utilized to construct receiver operating characteristic (ROC) curves for 2-, 3-, and 5-year outcomes within the training set. Kaplan–Meier (KM) survival curves were generated for both HRG and LRG using the "survminer" package (v 0.4.9).[29] Additionally, a risk triad plot was created to illustrate the expression levels of prognostic genes across different risk cohorts. Finally, the model was validated using the TCGA-THCA validation set and all tumor cohorts from TCGA-THCA to assess its efficacy.

2.5. Construction of a nomogram

In the training cohort, five clinical characteristics, namely age, stage, lymph node status (N), tumor size (T), and gender, were incorporated into the analysis. As the metastasis (M) stage had a large number of missing values, accounting for half of the sample, this indicator was excluded. To identify independent prognostic factors for THCA patients, univariate and multivariate Cox regression analyses were conducted on the aforementioned clinical characteristics in the TCGA-THCA training set. Subsequently, these independent prognostic factors were integrated with the risk score, and a nomogram was constructed using the "regplot" package (v 1.1)[30] to predict the survival rates of THCA patients at 2, 3, and 5 years. In addition, the calibration curve and ROC curve of the nomogram were plotted, and decision curve analysis (DCA) was conducted using the "ggDCA" package (v 1.2)[31] to evaluate the performance of the nomogram.

2.6. Evaluation of immune microenvironment and immunotherapy

The "CIBERSORT" package (v1.03)[32] was utilized to assess the differential levels of 22 immune cell types[33] between the HRG and LRG. Additionally, stacked bar plots and box plots representing the proportions of immune cells were generated using the "ggh4x" package (v 0.2.8).[34] Wilcoxon tests were performed to evaluate differences between the HRG and LRG. Furthermore, Spearman correlation analyses were conducted using the "psych" package (v 2.2.9)[35] to explore correlations between risk score and significantly different immune cell types. The correlation plots were generated using the "ggcor" package (v 0.9.7.4).[36] Furthermore, differential analysis was conducted on the expression levels of 68 immune checkpoint molecules, which included 20 immune-activating molecules, 21 immune-suppressing molecules, and 27 bidirectional molecules[37], to compare the HRG and LRG.

Tumor immune dysfunction and exclusion (TIDE) scores, interferon-gamma (IFNG) scores, exclusion scores, dysfunction scores, and myeloid-derived suppressor cell (MDSC) scores for cohorts in the TCGA-THCA training cohort were calculated via the TIDE framework (http://tide.dfci.harvard.edu/).[38] Differential comparisons between HRG and LRG were performed along with Wilcoxon tests. Additionally, Spearman correlation analysis was employed to investigate the relationships between risk score and TIDE scores. Furthermore, the correlations among risk score, TIDE scores, IFNG scores, exclusion scores, dysfunction scores, and MDSC scores were also assessed.

The immunophenoscore (IPS) was employed to evaluate the immunogenicity of various tumor types and their responses to immune checkpoint inhibitor (ICI) therapy. Data for the IPS were obtained from The Cancer Immunome Atlas (https://tcia.at/home). Subsequently, the Wilcoxon test was performed to compare responses between the HRG and LRG groups to anti-cytotoxic T-lymphocyte-associated protein 4 and anti-PD-1 blockade therapies.

2.7. Investigation of mutation landscape and drug sensitivity

The "maftools" package (v 2.17.10)[39] was utilized to analyze the gene mutation profiles within the TCGA-

THCA training cohort. Frequently mutated genes were identified in both the HRG and LRG, and a waterfall plot was generated to visually represent these mutations. Subsequently, commonly used chemotherapeutic agents for THCA patients were retrieved from the Genomics of Drug Sensitivity in Cancer database (http://cancerrxgene.org). The "oncoPredict" package (v 0.2)[40] was employed to calculate half-maximal inhibitory concentration (IC50) for these agents. Differences in IC50 values between the HRG and LRG were then compared.

2.8. Reverse transcription-quantitative polymerase chain reaction

In this study, five paired THCA tissues and adjacent non-tumor tissues were collected from patients at Shanxi Bethune Hospital to validate the expression of the prognostic genes. The study was approved by the Ethics Review Committee for Scientific Research, Shanxi Bethune Hospital (No: YXLL-2024-124). All experiments were performed in accordance with relevant guidelines and regulations, and consent was obtained from all participants and/or their legal guardians. Initially, 10–30 mg of each tissue sample was weighed to extract total RNA. Subsequently, the extracted RNA was reverse-transcribed into cDNA using the ABScript III RT Master Mix for reverse transcription (RT)-quantitative polymerase chain reaction (qPCR) with the gDNA remover kit (RK20429, ABclonal, USA). The cDNA was then subjected to RT-qPCR analysis using the Genious 2X SYBR Green Fast RT-qPCR Mix and run on an RT-qPCR system (RK21205, ABclonal, USA). Primers were designed using the Primer Premier (5.0, Premier Biosoft International, USA) (Table 1). After normalization of mRNA expression levels, relative expression levels were calculated using the $2^{-\Delta\Delta Ct}$ method.

2.9. Statistical analysis

R software was employed to conduct all analyses. The Wilcoxon test was employed to analyze the differences between the categories. $p < 0.05$ indicated statistical significance.

3. Results

3.1. Selection and enrichment analysis of differentially expressed liquid–liquid phase separation-related genes

In the training cohort of this study, differential analysis identified 4,144 DEGs between tumor and normal tissues, which included 2,415 upregulated genes and 1,729 downregulated genes (Figure 1A and 1B). An intersection with 1,065 LLPS-related genes revealed 75 differentially expressed LLPS-related genes in THCA (Figure 1C). The enrichment analysis revealed that these genes were associated with 1,173 GO terms. Notable terms included "regulation of protein modification by small protein conjugation or removal," "cytoplasmic side of plasma membrane," and "protein serine/threonine kinase activity" (Figure 1D). Furthermore, the differentially expressed LLPS-related genes were significantly involved in 29 KEGG pathways, such as the "MAPK signaling pathway," "PI3K-Akt signaling pathway," "estrogen signaling pathway," and "NF-kappa B signaling pathway" (Figure 1E). Additionally, the PPI network constructed from differentially expressed LLPS-related genes comprised 75 nodes and 155 interaction pairs. Within this network, key interactions involving *ESR1*, *APOE*, and *DLG4* were observed with multiple other genes (Figure 1F). In short, these findings identified candidate biomarkers and pathways potentially associated with THCA biology, providing a basis for subsequent functional investigation.

Table 1. Primer sequences

Gene	Sequence 5'–3'
GAPDH	F: 5'-GGAGTCCACTGGCGTCTTCA-3'
	R: 5'-GTCATGAGTCCTTCCACGATACC-3'
APOE	F: 5'-GTTGCTGGTCACATTCCTGG-3'
	R: 5'-GCAGGTAATCCCAAAAGCGAC-3'
ARHGEF4	F: 5'-CGAGCTGCTCAAATACACGC-3'
	R: 5'-TCTCCCTCCCAGTCCTCTATG-3'
CCL17	F: 5'-GTCTTGAAGCCTCCTCACCC-3'
	R: 5'-ATCTCCCTCACTGTGGCTCT-3'
DYRK3	F: 5'-ACAAACTTCGACAGTACGTGG-3'
	R: 5'-CAACTGGACGCTAAAACCCTG-3'
EGF	F: 5'-TGGATGTGCTTGATAAGCGG-3'
	R: 5'-ACCATGTCCTTTCCAGTGTGT-3'
HSPA1A	F: 5'-TAACCCCATCATCAGCGGAC-3'
	R: 5'-AGCTCCAAAACAAAAACAGCAA-3'
MAP1B	F: 5'-ATCTCGACACTCTGCAAGATTCT-3'
	R: 5'-TGTTTCTAAAACGTCACTTCGGT-3'

Abbreviations: F: Forward; R: Reverse.

3.2. Recognition of prognostic genes and construction of the risk model

A total of seven survival-related genes were identified using univariate Cox regression ($p < 0.05$) among the 75 differentially expressed LLPS-related genes (Figure 2A). These genes were subsequently integrated into an LASSO analysis, where the optimal model was achieved at lambda.

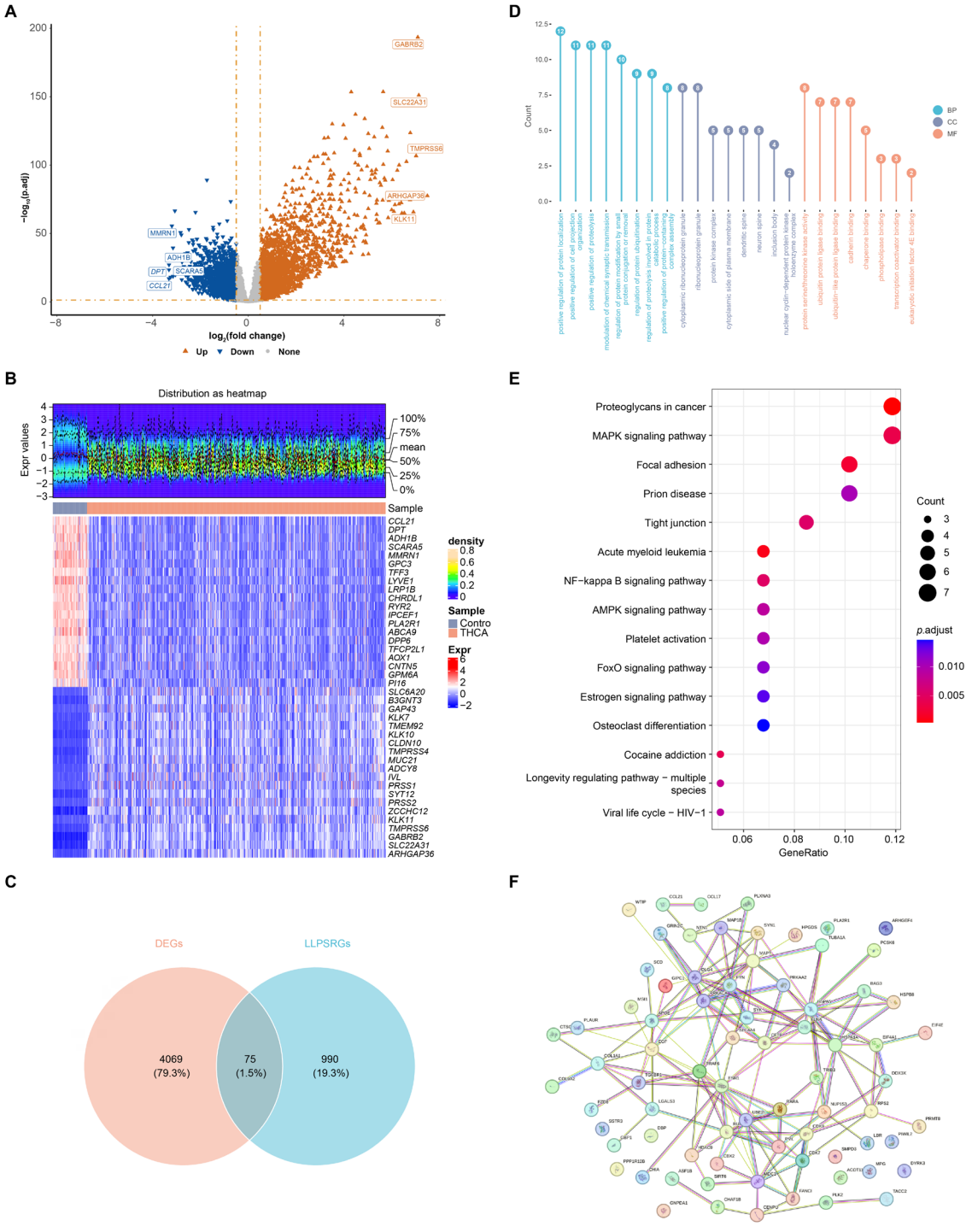

Figure 1. Identification and pathway analysis of differentially expressed LLPSRGs in the training cohort. (A, B) Volcano plot and heatmap of DEGs. (C) Venn diagram showing the intersection of DEGs with LLPSRGs to identify differentially expressed LLPSRGs. (D, E) Gene Ontology and Kyoto Encyclopedia of Genes and Genomes pathway enrichments among these differentially expressed LLPSRGs. (F) Visualization of the protein–protein interaction network for differentially expressed LLPSRGs.

Abbreviations: BP: Biological process; CC: Cellular component; DEGs: Differentially expressed genes; LLPSRGs: Liquid–liquid phase separation-related genes; MF: Molecular function; THCA: Thyroid carcinoma.

min = 0.003, resulting in the selection of seven prognostic genes: *APOE*, *ARHGEF4*, *CCL17*, *DYRK3*, *EGF*, *HSPA1A*, and *MAP1B* (Figure 2B). Afterward, in the training cohort, a risk model was developed using **Equation 1**:

$$\text{Risk score} = (-0.4056) \times APOE + (0.4192) \times ARHGEF4 + (0.4324) \times CCL17 + (0.9106) \times DYRK3 + (0.0921) \times EGF + (0.1455) \times HSPA1A + (0.2429) \times MAP1B \quad (1)$$

Under these circumstances, a series of additional analyses was conducted to validate the risk model. Specifically, the ROC curves for the risk model demonstrated area under the curve (AUC) values of 0.864, 0.806, and 0.793 at 2, 3, and 5 years, respectively, in the training cohort, indicating satisfactory predictive performance (Figure 2C). Furthermore, KM survival curves revealed significant differences in OS between the risk groups; the HRG exhibited significantly lower OS compared to the LRG within the training cohort ($p < 0.0001$) (Figure 2D). Additionally, the risk curve distinctly illustrated the distribution and survival status of THCA patients in both HRG and LRG. It was noted that the number of deaths in the HRG exceeded that in the LRG, indicating poorer survival for patients in the HRG (Figure 2E). Heatmap analysis further revealed that *APOE* showed lower expression in the HRG, whereas *ARHGEF4*, *CCL17*, *DYRK3*, *EGF*, *HSPA1A*, and *MAP1B* showed a trend of higher expression in this group (Figure 2F). Together, the effectiveness and reliability of the risk model were verified through a variety of analytical methods, providing strong support for its value in THCA research and clinical applications.

To further assess the model's universality, validation was conducted using the TCGA-THCA dataset (Figure 2G). The AUC values of the ROC curves were greater than 0.7 at 2-, 3-, and 5-year follow-up, indicating that the model exhibited satisfactory predictive performance. Furthermore, the mortality rate in the LRG was lower than in the HRG, and the expression trends of prognostic genes aligned with those observed in the training cohort. Similarly, additional validation was performed across all TCGA-THCA tumor cohorts (Figure 2H), yielding results consistent with those from both the training and validation cohorts. As a result, these discoveries offered compelling evidence of the prognostic model's predictive capabilities and suggested its applicability across different datasets.

3.3. Construction of the nomogram for predicting survival rates for thyroid carcinoma patients

To assess the independent prognostic significance of clinical characteristics in patients with THCA, five factors were incorporated into both univariate and multivariate Cox regression analyses. The findings confirmed that the risk score and age were recognized as independent prognostic factors. Specifically, the hazard ratio (HR) for risk score was 2.328 ($p < 0.01$), exceeding that for age, suggesting that risk score had a superior independent prognostic role compared to other clinicopathological factors (Figure 3A). Therefore, during subsequent diagnosis and treatment, the severity of the patient's condition can be predicted in advance based on the risk score, providing a crucial reference for the formulation of downstream treatment plans.

A nomogram was then constructed by integrating the risk score with other relevant clinicopathological factors, including age, N, T, and gender. The stage variable was excluded from the analysis due to multicollinearity identified during the Cox regression. The results demonstrated that predicted survival rates at 2, 3, and 5 years decreased as risk score increased, indicating that higher total scores correlated with lower survival rates (Figure 3B). Calibration curve analysis revealed that the slope of the curve approached 1 for predictions at 2, 3, and 5 years, suggesting that the model exhibited strong predictive capability (Figure 3C). To further validate the effectiveness of the predictive model, ROC and DCA curves were generated. The nomogram model achieved AUC values greater than 0.9 for predicting survival at 2, 3, and 5 years (Figure 3D), indicating exceptional overall performance. Additionally, DCA curves demonstrated favorable net benefits (Figure 3E, further substantiating the predictive ability of the nomogram model.

Through these analyses, this study established the risk score as a significant independent prognostic factor for patients with THCA and demonstrated the effectiveness of a nomogram constructed by integrating clinicopathological factors in predicting survival. These findings provide valuable insights for personalized treatment strategies in patients diagnosed with THCA.

3.4. Differences in the immune microenvironment between thyroid carcinoma patients with different risk levels

Significant differences in immune-cell composition were observed between risk groups, which may be associated with tumor progression and patient survival. The immune infiltration analysis revealed that among the 22 assessed cell types, seven exhibited significantly different infiltration levels between HRG and LRG ($p < 0.05$) (Figure 4A and 4B). Notably, the infiltration levels of several immune cells in tumor tissues, specifically "resting memory CD4 T cells," "gamma delta T cells," "macrophages," "activated

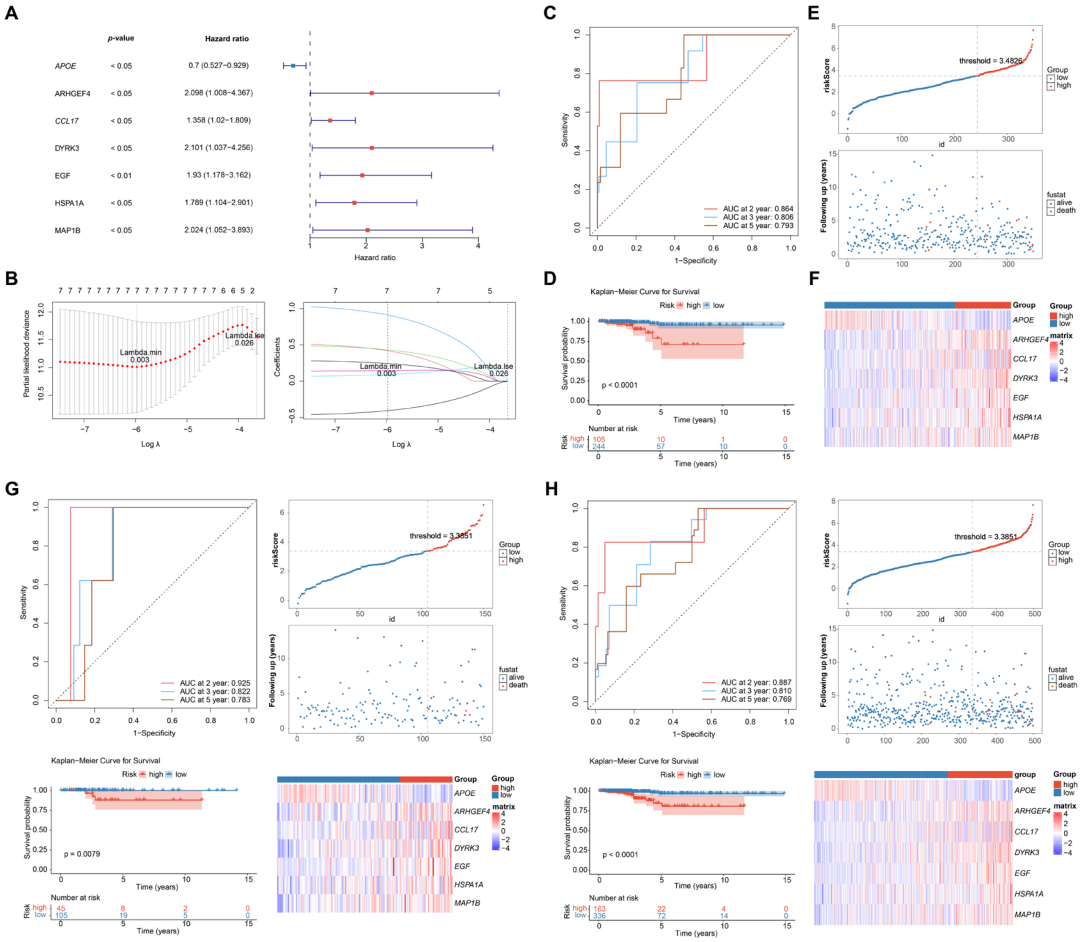

Figure 2. Identification of prognostic genes and construction of a risk model for THCA. (A) Univariate Cox regression screening for prognostic genes. (B) Least Absolute Shrinkage and Selection Operator regression analysis applied to prognostic genes identified via univariate Cox regression in the training cohort. (C) Receiver operating characteristic curves of the risk model, with AUC calculated for 2-, 3-, and 5-year follow-up in the training cohort. (D) Kaplan–Meier survival curves showing differences in overall survival between HRG and LRG in the training cohort. (E) Risk curves illustrating the distribution of risk scores and survival status among HRG and LRG in the training cohort. (F) Heatmaps displaying the expression patterns of prognostic genes across HRG and LRG in the training cohort. (G) Validation of models in the TCGA-THCA testing set. (H) Validation of models in the entire TCGA-THCA cohort.

Abbreviations: AUC: Area under the curve; HRG: High-risk group; LRG: Low-risk group; TCGA: The Cancer Genome Atlas; THCA: Thyroid carcinoma.

dendritic cells," and "eosinophils," were significantly elevated. Conversely, the infiltration levels of "M0 and M2 macrophages" were found to be lower in tumor tissues. Correlation analysis indicated that "resting memory CD4 T cells" exhibited the strongest positive correlation with risk score (cor = 0.298, $p < 0.05$), while "gamma delta T cells" demonstrated the strongest negative correlation (cor = −0.196, $p < 0.05$) (Figure 4C). These findings suggested that "resting memory CD4 T cells" may facilitate tumor progression and increase patient risk, whereas "gamma delta T cells" may suppress tumor growth and reduce patient risk.

Furthermore, a differential expression analysis of 68 immune checkpoint molecules was conducted to further investigate the differences in immune characteristics between HRG and LRG. The results demonstrated significant differences in the expression levels of four immune-activating, seven immune-suppressing, and nine bidirectional immune checkpoint molecules between the two groups (Figure 4D). The identification of these significantly different immune checkpoint molecules provided crucial targets for the formulation of subsequent precise immunotherapy strategies.

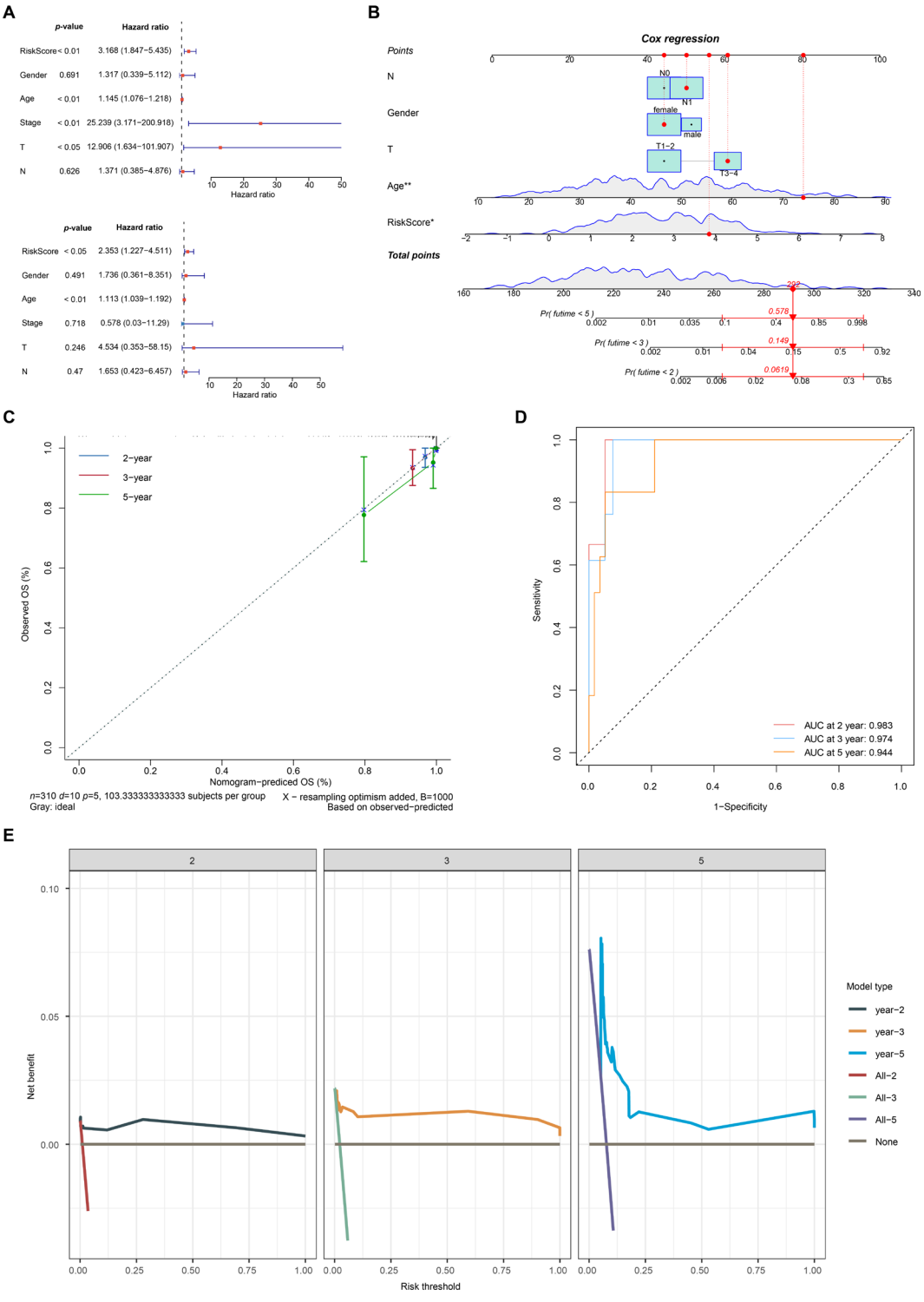

Figure 3. Identification of independent prognostic factors and construction of a nomogram in the training cohort. (A) Univariate and multivariate Cox regression analysis to identify independent prognostic factors. (B) Construction of a nomogram based on the clinical factors and risk scores. (C) Calibration curve for the nomogram. (D) Receiver operating characteristic curve for the nomogram. (E) Decision curve analysis for the nomogram.
Notes: *$p < 0.05$; **$p < 0.01$.
Abbreviations: AUC: Area under the curve; N: Lymph node status; OS: Overall survival; T: Tumor size.

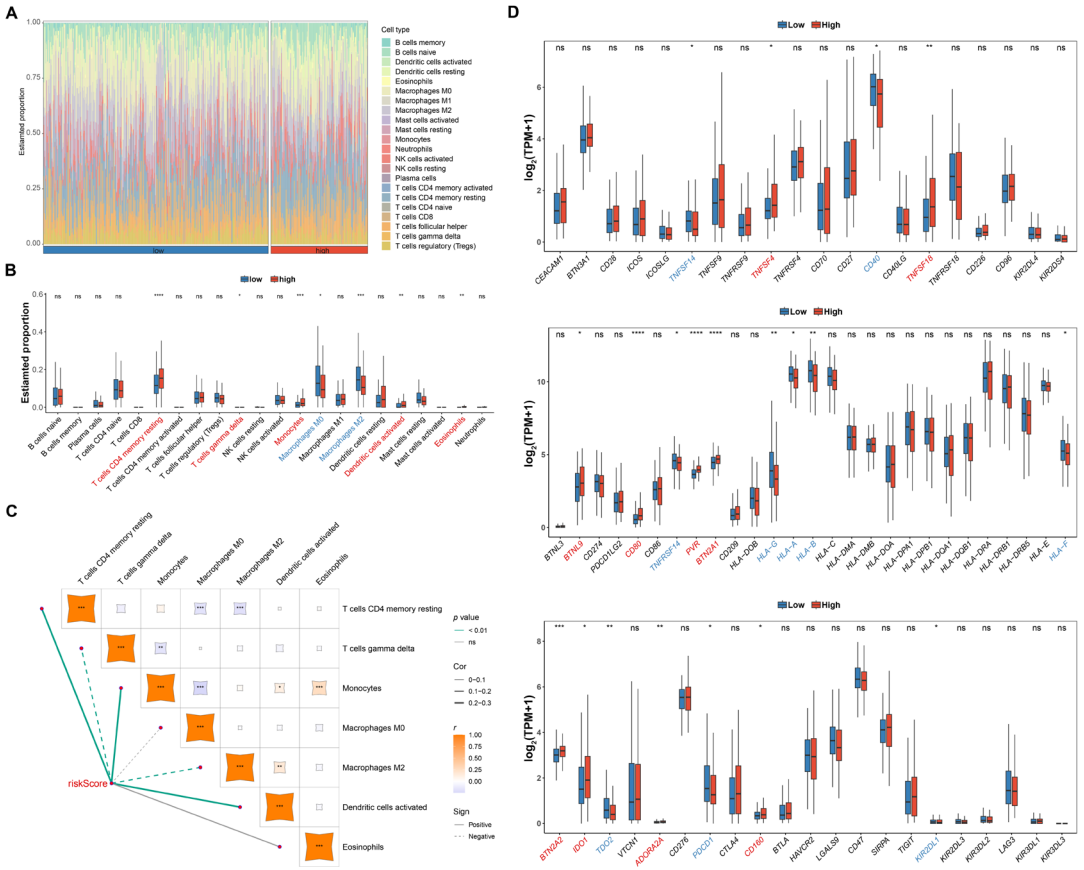

Figure 4. Analysis of the immune function in the training cohort. (A) The infiltration abundance of 22 immune cell types. (B) Differences in the infiltration abundance of 22 immune cell types between the HRG and LRG. (C) Correlation between differentially infiltrating immune-cell types and the risk score. (D) Comparison of the immune-checkpoint genes in the HRG and LRG.
Notes: *$p < 0.05$; **$p < 0.01$; ***$p < 0.001$; ****$p < 0.0001$; ns: $p > 0.05$.
Abbreviations: HRG: High-risk group; LRG: Low-risk group; TPM: Transcripts per million.

Subsequently, TIDE analysis was performed on THCA-tumor cohorts to assess the potential for immune evasion. The results indicated a positive correlation between risk score and TIDE score, with HRG exhibiting higher TIDE scores than LRG (Figure 5A). It indicated that the higher a patient's risk score, the greater the likelihood of immune evasion by their tumor cells. Furthermore, correlation analyses conducted on cohorts from the TCGA-THCA training cohort revealed relationships among risk score, TIDE, IFNG, exclusion, dysfunction, and MDSC. Exclusion demonstrated the highest correlation with MDSC (cor = 0.78, $p < 0.05$), followed by Dysfunction with IFNG (cor = 0.64, $p < 0.05$) (Figure 5B). Finally, an analysis of responses to ICI therapy revealed that four IPS scores-ips_ctla4_neg_pd1_neg, ips_ctla4_neg_pd1_pos, ips_ctla4_pos_pd1_pos, and ips_ctla4_pos_pd1_neg-were significantly increased in the LRG (Figure 5C).

3.5. Assessment of mutation genes and IC50 differences of chemotherapy drugs between high- and low-risk groups

To investigate primary gene mutations across risk groups, an analysis of tumor gene mutations in the TCGA-THCA training cohort was conducted. The results displayed that the top three genes with the greatest alteration frequencies in the LRG were *BRAF*, *NRAS*, and *TG*, whereas the top three mutated genes in the HRG were *BRAF*, *NRAS*, and *TTN* (Figure 6A). Subsequently, the IC50s of 198 chemotherapeutic agents were compared between HRG and LRG. Among these agents, 51 showed statistically significant differences, including P22077_1933, AZD1208_1449, Nilotinib_1013, and others (Figure

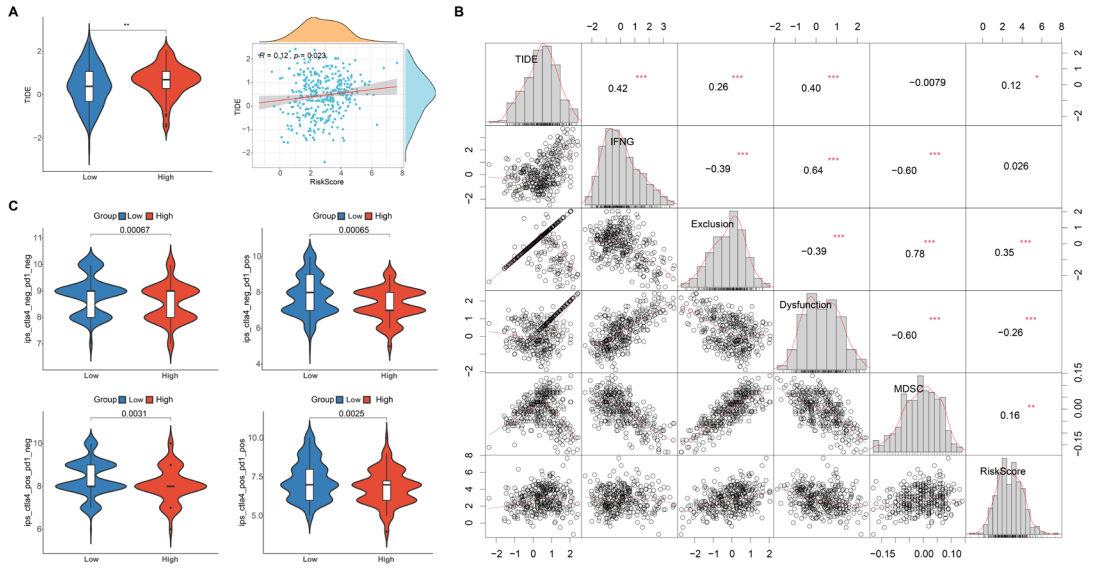

Figure 5. Immune escape sensitivity in the training cohort. (A) Analysis of immune escape in the HRG and LRG. (B) Correlation between risk score, TIDE scores, Interferon-gamma (IFNG) scores, Exclusion scores, and myeloid-derived suppressor cell scores. (C) Violin plots showing the relationship between immunophenoscore and risk groups.
Abbreviations: HRG: High-risk group; LRG: Low-risk group; TIDE: Tumor Immune Dysfunction and Exclusion.

S1). This finding suggests that these 51 drugs may exert differential therapeutic effects on patients at various stages of tumor progression.

Furthermore, an analysis was conducted on the IC50 differences of commonly used chemotherapy agents for THCA, including paclitaxel (Paclitaxel_1080), cisplatin (Cisplatin_1005), cyclophosphamide (Cyclophosphamide_1512), and 5-fluorouracil (5-Fluorouracil_1073) between the HRG and LRG. The correlation between risk score and the IC50 values of these four chemotherapy drugs was also calculated. Notably, significant differences in the IC50 values of both paclitaxel and cyclophosphamide were observed between HRG and LRG (Figure 6B). These results could help clinicians predict patients' responses to specific chemotherapeutic drugs based on risk groups before formulating chemotherapy regimens, thereby enabling personalized treatment and improving the precision and effectiveness of chemotherapy.

3.6. Expression of prognostic genes in thyroid carcinoma

In this study, the expression levels of prognostic genes were verified using RT-qPCR. The results demonstrated that, compared to the normal control group, the expression levels of *APOE*, *ARHGEF4*, *CCL17*, *DYRK3*, *HSPA1A*, and *MAP1B* were significantly upregulated in the THCA group, while *EGF* was significantly downregulated (Figure S2). Notably, RT-qPCR results for these four prognostic genes—*APOE*, *CCL17*, *MAP1B*, and *EGF*—were highly consistent with those of the previous bioinformatics analysis. This not only further validated the reliability of the research data but also provided strong evidence in support of the in-depth exploration of the pathogenesis of THCA and the prognostic evaluation.

4. Discussion

The critical function of LLPS in the formation of membraneless organelles has garnered increasing attention in recent years.[41] By modulating cellular processes such as signal transduction, gene expression, and stress responses, these dynamic structures play significant roles in tumorigenesis.[42] The characteristics of LLPS-related genes have been shown to be prognostic markers and predictors of therapeutic response in esophageal adenocarcinoma research.[43] It is important to note that LLPS provides new insights into the adaptability of tumor cells by effectively regulating the mitogen-activated protein kinase pathway by sequestering signaling molecules such as protein kinase C/phosphoenolpyruvate carboxykinase 2 within stress granules.[44] It has been confirmed that dysregulation of LLPS, which results in cellular dysfunction, is associated with a variety of cancers[45]; however, its significance in THCA is still unexplored.

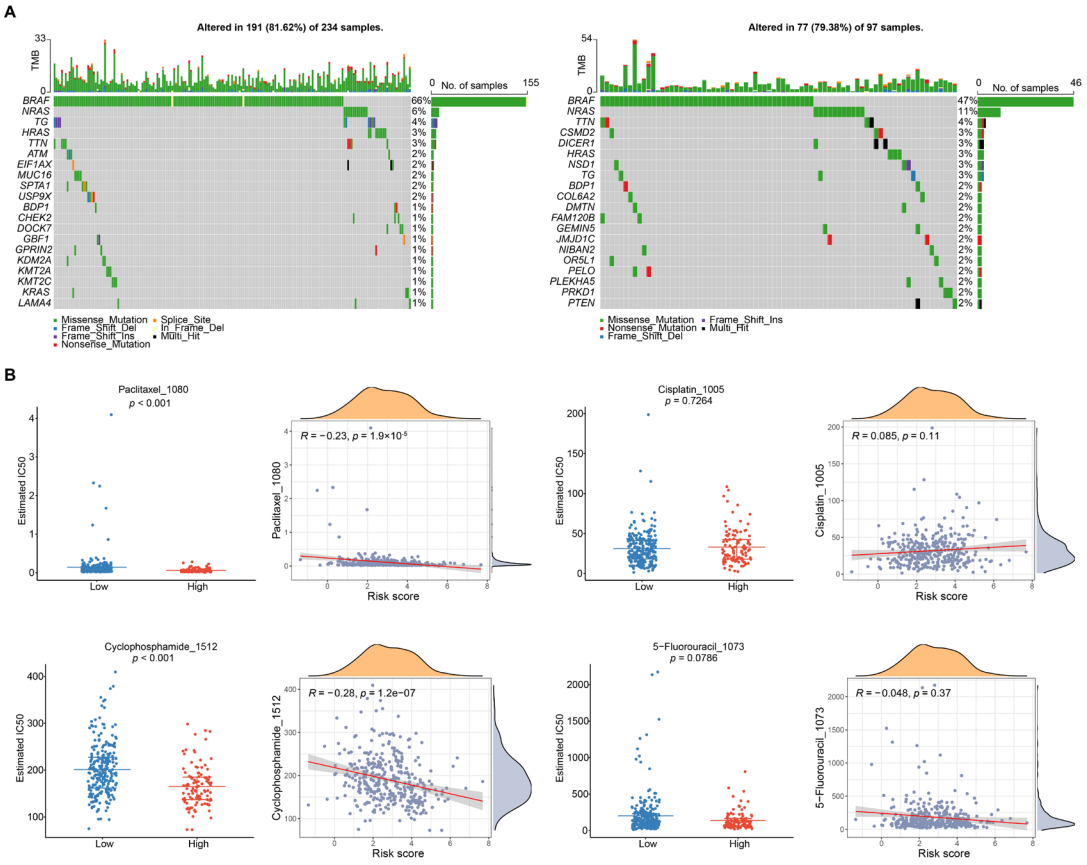

Figure 6. Mutation and drug sensitivity analysis. (A) Somatic mutation profile in HRG and LRG. (B) Variations in IC50 values of common chemotherapeutic drugs between the HRG and LRG.
Notes: *$p < 0.05$; **$p < 0.01$; ***$p < 0.001$; ****$p < 0.0001$; ns: $p > 0.05$.
Abbreviations: HRG: High-risk group; IC50: Half-maximal inhibitory concentration; LRG: Low-risk group.

The present investigation innovatively identified seven LLPS-related prognostic genes in THCA (*APOE*, *ARHGEF4*, *CCL17*, *DYRK3*, *EGF*, *HSPA1A*, and *MAP1B*) and developed a risk model with a robust predictive efficacy. The risk score (HR = 2.328) served as a stronger independent prognostic factor than age, as shown by multivariate Cox regression analysis. The patient's survival rates are precisely predicted by the nomogram developed using this score. Experimental validation further confirmed the upregulation of *APOE*, *CCL17*, and *MAP1B* and the downregulation of *EGF* in disease groups, which was consistent with the bioinformatics findings. However, although these genes are cataloged as LLPS-related in DrLLPS, the present study does not demonstrate that their prognostic effects in THCA are mediated through LLPS-dependent mechanisms. Their relevance to THCA may involve LLPS-associated biology, non-LLPS functions, or both.

Apolipoprotein E (APOE) is a major cholesterol carrier in the brain and is essential for a variety of cellular processes, such as neuroinflammation, the degradation and clearance of β-amyloid, synaptogenesis, membrane repair and remodeling, and neuronal growth.[46] In recent years, research on APOE has expanded from neurological disorders to the field of cancer, revealing its potential function in the initiation and progression of tumors.[47] Notably, polymorphisms of the *APOE* gene, including rs429358 and rs7412, have been demonstrated to be closely associated with the risk of developing THCA. In particular, rs429358 has been identified as a risk variant for THCA, whereas rs7412 demonstrates a protective effect. This suggests that *APOE* may be involved in the pathogenesis of THCA by regulating cellular lipid metabolism and ferroptosis processes.[48] Additionally, APOE induces the polarization of tumor-associated macrophages from the M0 phenotype to the M2 phenotype and regulates the

expression of inflammatory factors via the phosphoinositide 3-kinase (PI3K)/protein kinase B (Akt)/nuclear factor kappa B (NF-κB) signaling pathway. In the development and occurrence of PTC, this mechanism is significant.[49] As our study has shown, *APOE* is predominantly highly expressed in the LRG, which further supports its potential as a therapeutic target for patients at low risk of THCA.

Silencing dual-specificity tyrosine-(Y)-phosphorylation-regulated kinase 3 (DYRK3), a dual-specificity kinase, has been shown to inhibit the migratory and invasion abilities of tumor cells.[50] This phenomenon highlights the important role of DYRK3 in the development process of tumors. For example, in glioblastoma, DYRK3 enhances tumor invasiveness by modifying mitochondrial morphology and function.[51] Furthermore, DYRK3 has been associated with poor prognosis as an oncogene in serous ovarian cancer.[52] However, there remains a scarcity of research on DYRK3 specifically in THCA. Moreover, epidermal growth factor (EGF) and its receptor (EGFR) are closely associated with the occurrence and development of various tumors.[53] In thyroid anaplastic carcinoma cells (SUN-80), EGF activates the EGFR signaling pathway in a time- and dose-dependent manner. This process involves clathrin-, Rab5/7- and early endosome antigen 1-mediated EGFR internalization and trafficking, induces EGFR nuclear translocation, subsequently modulates cell cycle progression, and ultimately promotes SUN-80 cell proliferation and migration.[54] Additionally, fucosyltransferase VII promotes the malignant transformation of follicular THCA via α1,3-fucosylation of the EGF receptor.[55]

Another important factor is heat shock protein family A member 1A (HSPA1A), which is encoded by the *HSPA1A* gene.[56] Studies have demonstrated that heat shock proteins, as overexpressed molecular chaperones in thyroid malignancies, are involved in key functions such as apoptosis protection, drug resistance, and cell migration, and have therefore been proposed as novel therapeutic targets for THCA to reverse the molecular mechanisms of tumor progression.[57] Furthermore, the differential expression of *HSPA1A* in thyroid tissues suggests that it has the potential to serve as a diagnostic and prognostic biomarker for cancer.[58] C-C motif chemokine ligand 17 (CCL17) is another chemokine regulated by thymus activation that influences immune cell infiltration into the tumor microenvironment across various malignant tumors.[59] This infiltration contributes to tumor invasion and metastasis; indeed, elevated expression of *CCL17* in THCA has been associated with poorer survival outcomes, underscoring its potential as a prognostic biomarker for tumor immunity.[60] Lastly, while rho guanine nucleotide exchange factor 4 (ARHGEF4) is highly expressed in pancreatic cancer and is associated with poor OS[61], and microtubule-associated protein 1B (MAP1B) is highly expressed in triple-negative breast cancer[62], neither of these genes has been investigated in the context of THCA. In conclusion, our identification of these prognostic genes highlights their significance not only for understanding the underlying mechanisms of THCA but also for developing novel therapeutic strategies aimed at improving patient outcomes.

Our immune microenvironment analysis showed that the LLPS-related risk signature was associated with differences in immune-cell infiltration, immune checkpoint molecule expression, TIDE-related immune evasion scores, IFNG-related features, MDSC scores, and predicted ICI responsiveness. These results suggest a potential association between the prognostic signature and immune-related features in THCA. Among the seven prognostic genes, *CCL17* may be particularly relevant, as it is a chemokine involved in immune-cell recruitment and has been associated with tumor immunity and poorer survival outcomes in THCA.[60,63,64] *APOE* may also be related to immune regulation through macrophage polarization and inflammatory signaling via the PI3K/Akt/NF-κB pathway.[49,65] In addition, *HSPA1A* may be involved in stress-related inflammatory responses[66], while EGF/EGFR-related signaling has been implicated in thyroid cancer progression.[67] These observations may partly explain the immune differences observed between HRG and LRG. However, for *ARHGEF4*, *DYRK3*, and *MAP1B*, direct evidence linking them to immune checkpoints or cytokine regulation in THCA remains limited. Moreover, because our analysis was based on bulk transcriptomic data, it cannot determine the cell-type-specific sources of these genes or prove direct regulatory relationships between these genes and immune checkpoints or cytokines. Future studies using single-cell sequencing, spatial transcriptomics, and functional experiments are needed to clarify these mechanisms.

Our pharmacogenomic analysis revealed significant differences in IC50 values for conventional chemotherapeutic agents between HRG and LRG groups. Notably, paclitaxel and cyclophosphamide showed marked differences in IC50 values across these risk stratifications. As a broad-spectrum antineoplastic agent, paclitaxel has demonstrated robust antitumor efficacy across multiple malignancies.[68,69] Mechanistic studies indicate that ultrasound-targeted microbubble destruction-mediated miR-144-5p overexpression enhances paclitaxel's therapeutic effects in THCA through stonin 2 targeting.[69] Furthermore, extended paclitaxel administration has

shown favorable clinical outcomes in primary thyroid squamous cell carcinoma management[70], reinforcing its potential utility in thyroid oncology.

Our study delves into the prognostic genes of THCA within the context of LLPS, successfully identifying LLPS-related prognostic genes and constructing a risk model. This model demonstrates strong predictive performance for THCA patient survival and reveals differences in the immune microenvironment between HRG and LRG, as well as their impacts on immunotherapy, thereby providing a basis for personalized treatment. The main contribution of this study is the construction of a transcriptome-based prognostic framework centered on LLPS-related genes in THCA. This framework may facilitate risk stratification and provide candidate genes for future mechanistic studies exploring whether and how LLPS-associated processes participate in THCA biology.

However, several limitations should be acknowledged. First, this study is retrospective and primarily relies on a public cohort (TCGA-THCA). Because THCA generally has an excellent prognosis, the number of observed outcome events is limited, especially after splitting the dataset into training and validation cohorts. This small event count may compromise model stability and may lead to optimistic performance estimates. Although we applied penalized LASSO-Cox regression with cross-validation and observed broadly consistent discrimination and risk stratification across the training set, validation set, and the entire cohort, independent validation in larger multicenter cohorts with longer follow-up remains necessary to confirm robustness and clinical utility. Second, functional and mechanistic experiments were not performed, including gene knockdown or overexpression assays in THCA cell lines and direct assessment of droplet formation, condensate dynamics, or other phase-separation-related phenotypes. In addition, the RT-qPCR validation was based on a limited number of paired clinical tissue samples, and the relatively small clinical sample size may not fully account for the inherent heterogeneity of THCA. Therefore, future studies with larger clinical sample sizes are needed to further validate the expression patterns of the identified genes and the robustness of the proposed risk model. Accordingly, the present findings should be interpreted as transcriptome-based associations rather than direct evidence that LLPS drives THCA progression or prognosis. Third, the designation of "LLPS-related genes" in this study was based on public database annotation rather than direct experimental assessment in THCA tissues or cells. Therefore, our data do not demonstrate that LLPS events actually occur in THCA, nor do they establish that the prognostic effects of these genes are mediated through LLPS-dependent mechanisms. Further studies incorporating direct assays of LLPS-related phenomena are needed to determine whether and how LLPS contributes to THCA pathogenesis. Fourth, drug sensitivity was inferred from pharmacogenomic prediction models and lacks direct clinical or experimental confirmation; prospective studies and therapeutic validation are needed. Taken together, despite these limitations, our findings provide a transcriptome-based prognostic framework based on genes annotated as LLPS-related and associated with THCA outcomes and may support future risk stratification and personalized management while generating hypotheses for subsequent mechanistic investigation.

5. Conclusion

In conclusion, this study identified seven prognostic genes annotated as LLPS-related in THCA and established a transcriptome-based risk model with favorable predictive performance. The prognostic signature was further associated with differences in immune infiltration and predicted drug sensitivity, suggesting its potential relevance for risk stratification. These findings provide candidate biomarkers and a hypothesis-generating framework for THCA research, although the mechanistic involvement of LLPS in THCA remains to be established by future experimental studies.

Acknowledgments

The authors thank the Department of Thyroid Surgery and Bariatric Metabolic Surgery and the Department of Blood Transfusion at Shanxi Bethune Hospital for their support.

Funding

None.

Conflict of interest

The authors declare they have no competing interests.

Author contributions

Conceptualization: Wenjun Zhao, Peng Ma
Formal analysis: All authors
Investigation: All authors
Methodology: All authors
Writing–original draft: Jian Wang, Lei Zhang
Writing–review & editing: All authors

Ethics approval and consent to participate

This study was performed in line with the principles of the Declaration of Helsinki. Approval was granted by the Ethics Review Committee for Scientific Research, Shanxi Bethune Hospital (No: YXLL-2024-124).

Consent for publication

Informed consent was obtained from all individual participants included in the study.

Availability of data

The datasets analyzed during the current study are available in the University of California, Santa Cruz Xena database (https://xenabrowser.net/datapages/, TCGA-THCA dataset).

References

1. Kim JY, Myung JK, Kim S, Tae K, Choi YY, Lee SJ. Prognosis of poorly differentiated thyroid carcinoma: a systematic review and meta-analysis. *Endocrinol Metab*. 2024;39(4):590-602.

   doi: 10.3803/EnM.2024.1927

2. Liu Q, Sun W, Zhang H. Roles and new insights of macrophages in the tumor microenvironment of thyroid cancer. *Front Pharmacol*. 2022;13:875384.

   doi: 10.3389/fphar.2022.875384

3. Chen DW, Lang BHH, McLeod DSA, Newbold K, Haymart MR. Thyroid cancer. *Lancet*. 2023;401(10387):1531-1544.

   doi: 10.1016/s0140-6736(23)00020-x

4. Shobab L, Burman KD, Wartofsky L. Sex differences in differentiated thyroid cancer. *Thyroid*. 2022;32(3):224-235.

   doi: 10.1089/thy.2021.0361

5. Fuloria S, Subramaniyan V, Karupiah S, *et al*. Comprehensive review of methodology to detect reactive oxygen species (ROS) in mammalian species and establish its relationship with antioxidants and cancer. *Antioxidants*. 2021;10(1):128.

   doi: 10.3390/antiox10010128

6. Jaume JC. Thyroid cancer—the tumor immune microenvironment (TIME) over time and space. *Cancers*. 2025;17(5):794.

   doi: 10.3390/cancers17050794

7. Xie Z, Li X, He Y, *et al*. Immune cell confrontation in the papillary thyroid carcinoma microenvironment. *Front Endocrinol*. 2020;11:570604.

   doi: 10.3389/fendo.2020.570604

8. Bergdorf K, Ferguson DC, Mehrad M, Ely K, Stricker T, Weiss VL. Papillary thyroid carcinoma behavior: clues in the tumor microenvironment. *Endocr Relat Cancer*. 2019;26(6):601-614.

   doi: 10.1530/erc-19-0074

9. Wang B, Zhang L, Dai T, *et al*. Liquid-liquid phase separation in human health and diseases. *Signal Transduct Target Ther*. 2021;6(1):290.

   doi: 10.1038/s41392-021-00678-1

10. Lv L, Zhang X, Liu Y, Zhu X, Pan R, Huang L. Three liquid-liquid phase separation-related genes associated with prognosis in glioma. *Pharmgenomics Pers Med*. 2024;17:171-181.

    doi: 10.2147/pgpm.S442000

11. Bracha D, Walls MT, Brangwynne CP. Probing and engineering liquid-phase organelles. *Nat Biotechnol*. 2019;37(12):1435-1445.

    doi: 10.1038/s41587-019-0341-6

12. Mehta S, Zhang J. Liquid-liquid phase separation drives cellular function and dysfunction in cancer. *Nat Rev Cancer*. 2022;22(4):239-252.

    doi: 10.1038/s41568-022-00444-7

13. Tong X, Tang R, Xu J, *et al*. Liquid-liquid phase separation in tumor biology. *Signal Transduct Target Ther*. 2022;7(1):221.

    doi: 10.1038/s41392-022-01076-x

14. Mao S, Liu Q, Wu H, *et al*. Phase separation of YAP mediated by coiled-coil domain promotes hepatoblastoma proliferation via activation of transcription. *J Gastroenterol Hepatol*. 2023;38(8):1398-1407.

    doi: 10.1111/jgh.16173

15. Liu J, Liu ZX, Li JJ, *et al*. The macrophage-associated lncRNA MALR facilitates ILF3 liquid-liquid phase separation to promote HIF1α signaling in esophageal cancer. *Cancer Res*. 2023;83(9):1476-1489.

    doi: 10.1158/0008-5472.Can-22-1922

16. Xie J, Chen L, Wu D, *et al*. Significance of liquid-liquid phase separation (LLPS)-related genes in breast cancer: a multi-omics analysis. *Aging*. 2023;15(12):5592-5610.

    doi: 10.18632/aging.204812

17. You Q, Chen JY, Wu XH, *et al*. A liquid-liquid phase separation-related index associate with biochemical recurrence and tumor immune environment of prostate cancer patients. *Int J Mol Sci*. 2023;24(6):5515.

    doi: 10.3390/ijms24065515

18. Tang Q, Mao X, Chen Z, *et al*. Liquid-liquid phase separation-related gene in gliomas: FABP5 is a potential prognostic marker. *J Gene Med*. 2023;25(10):e3517.

    doi: 10.1002/jgm.3517

19. Love MI, Huber W, Anders S. Moderated estimation of fold change and dispersion for RNA-seq data with DESeq2. *Genome Biol*. 2014;15(12):550.

    doi: 10.1186/s13059-014-0550-8

20. Gustavsson EK, Zhang D, Reynolds RH, Garcia-Ruiz S, Ryten M. ggtranscript: an R package for the visualization and interpretation of transcript isoforms using ggplot2. *Bioinformatics*. 2022;38(15):3844-3846.

    doi: 10.1093/bioinformatics/btac409

21. Gu Z, Hübschmann D. Make interactive complex heatmaps in R. *Bioinformatics*. 2022;38(5):1460-1462.

    doi: 10.1093/bioinformatics/btab806

22. Chen H, Boutros PC. VennDiagram: a package for the generation of highly-customizable Venn and Euler diagrams in R. *BMC Bioinform*. 2011;12(1):35.

    doi: 10.1186/1471-2105-12-35

23. Yu G, Wang LG, Han Y, He QY. clusterProfiler: an R package for comparing biological themes among gene clusters. *OMICS*. 2012;16(5):284-287.

    doi: 10.1089/omi.2011.0118

24. Zhuge L, Zhang K, Zhang Z, Guo W, Li Y, Bao Q. A novel model based on liquid-liquid phase separation-related genes correlates immune microenvironment profiles and predicts prognosis of lung squamous cell carcinoma. *J Clin Lab Anal*. 2022;36(1):e24135.

    doi: 10.1002/jcla.24135

25. Liu P, Xu H, Shi Y, Deng L, Chen X. Potential molecular mechanisms of plantain in the treatment of gout and hyperuricemia based on network pharmacology. *Evid Based Complement Alternat Med*. 2020;2020:3023127.

    doi: 10.1155/2020/3023127

26. Lei J, Qu T, Cha L, *et al*. Clinicopathological characteristics of pheochromocytoma/paraganglioma and screening of prognostic markers. *J Surg Oncol*. 2023;128(4):510-518.

    doi: 10.1002/jso.27358

27. Li Y, Lu F, Yin Y. Applying logistic LASSO regression for the diagnosis of atypical Crohn's disease. *Sci Rep*. 2022;12(1):11340.

    doi: 10.1038/s41598-022-15609-5

28. Heagerty PJ, Lumley T, Pepe MS. Time-dependent ROC curves for censored survival data and a diagnostic marker. *Biometrics*. 2000;56(2):337-344.

    doi: 10.1111/j.0006-341x.2000.00337.x

29. Ramsay IS, Ma S, Fisher M, *et al*. Model selection and prediction of outcomes in recent onset schizophrenia patients who undergo cognitive training. *Schizophr Res Cogn*. 2018;11:1-5.

    doi: 10.1016/j.scog.2017.10.001

30. Yu H, Ji X, Ouyang Y. Unfolded protein response pathways in stroke patients: a comprehensive landscape assessed through machine learning algorithms and experimental verification. *J Transl Med*. 2023;21(1):759.

    doi: 10.1186/s12967-023-04567-9

31. Zhao S, Chi H, Yang Q, *et al*. Identification and validation of neurotrophic factor-related gene signatures in glioblastoma and Parkinson's disease. *Front Immunol*. 2023;14:1090040.

    doi: 10.3389/fimmu.2023.1090040

32. Chen B, Khodadoust MS, Liu CL, Newman AM, Alizadeh AA. Profiling tumor infiltrating immune cells with CIBERSORT. *Methods Mol Biol*. 2018;1711:243-259.

    doi: 10.1007/978-1-4939-7493-1_12

33. Newman AM, Liu CL, Green MR, *et al*. Robust enumeration of cell subsets from tissue expression profiles. *Nat Methods*. 2015;12(5):453-457.

    doi: 10.1038/nmeth.3337

34. Feng X, Qin S, Zhang D, *et al*. Nitrogen input enhances microbial carbon use efficiency by altering plant-microbe-mineral interactions. *Glob Chang Biol*. 2022;28(16):4845-4860.

    doi: 10.1111/gcb.16229

35. Robles-Jimenez LE, Aranda-Aguirre E, Castelan-Ortega OA, *et al*. Worldwide traceability of antibiotic residues from livestock in wastewater and soil: a systematic review. *Animals*. 2022;12(1):60.

    doi: 10.3390/ani12010060

36. Bahram M, Hildebrand F, Forslund SK, *et al*. Structure and function of the global topsoil microbiome. *Nature*. 2018;560(7717):233-237.

    doi: 10.1038/s41586-018-0386-6

37. Hu FF, Liu CJ, Liu LL, Zhang Q, Guo AY. Expression profile of immune checkpoint genes and their roles in predicting immunotherapy response. *Brief Bioinform*. 2021;22(3):bbaa176.

    doi: 10.1093/bib/bbaa176

38. Jiang P, Gu S, Pan D, *et al*. Signatures of T cell dysfunction and exclusion predict cancer immunotherapy response. *Nat Med*. 2018;24(10):1550-1558.

    doi: 10.1038/s41591-018-0136-1

39. Mayakonda A, Lin DC, Assenov Y, Plass C, Koeffler HP. Maftools: efficient and comprehensive analysis of somatic variants in cancer. *Genome Res*. 2018;28(11):1747-1756.

    doi: 10.1101/gr.239244.118

40. Maeser D, Gruener RF, Huang RS. oncoPredict: an R package for predicting in vivo or cancer patient drug response and biomarkers from cell line screening data. *Brief Bioinform*. 2021;22(6):bbab260.

    doi: 10.1093/bib/bbab260

41. Hu YQ, Li PP, Sun K, Yang KX, Zhang WJ, Wu ZY. Comprehensive analysis of liquid-liquid phase separation-related genes in prediction of breast cancer prognosis. *Front Genet*. 2022;13:834471.

    doi: 10.3389/fgene.2022.834471

42. Liu Z, Qin Z, Liu Y, *et al*. Liquid–liquid phase separation: roles and implications in future cancer treatment. *Int J Biol Sci*. 2023;19(13):4139-4156.

doi: 10.7150/ijbs.81521

43. Tao B, Wang F, Zhu L. Liquid-liquid phase separation-related signature predicts prognosis and therapeutic response in esophageal adenocarcinoma. *Anal Chim Acta*. 2024;1330:343202.

doi: 10.1016/j.aca.2024.343202

44. Sugiura R. Stress granules safeguard against MAPK signaling hyperactivation by sequestering PKC/Pck2: new findings and perspectives. *Curr Genet*. 2021;67(6):857-863.

doi: 10.1007/s00294-021-01192-1

45. Zhang JZ, Mehta S, Zhang J. Liquid-liquid phase separation: a principal organizer of the cell's biochemical activity architecture. *Trends Pharmacol Sci*. 2021;42(10):845-856.

doi: 10.1016/j.tips.2021.07.003

46. Serrano-Pozo A, Das S, Hyman BT. APOE and Alzheimer's disease: advances in genetics, pathophysiology, and therapeutic approaches. *Lancet Neurol*. 2021;20(1):68-80.

doi: 10.1016/s1474-4422(20)30412-9

47. Ostendorf BN, Bilanovic J, Adaku N, *et al*. Common germline variants of the human APOE gene modulate melanoma progression and survival. *Nat Med*. 2020;26(7):1048-1053.

doi: 10.1038/s41591-020-0879-3

48. Xiao Z, Zhao H. Ferroptosis-related APOE, BCL3 and ALOX5AP gene polymorphisms are associated with the risk of thyroid cancer. *Pharmgenomics Pers Med*. 2022;15:157-165.

doi: 10.2147/pgpm.S352225

49. Huo R, Zhao R, Li Z, *et al*. APOE expression in papillary thyroid carcinoma: influencing tumor progression and macrophage polarization. *Immunobiology*. 2024;229(5):152821.

doi: 10.1016/j.imbio.2024.152821

50. Ramella M, Ribolla LM, Surini S, *et al*. Dual specificity kinase DYRK3 regulates cell migration by influencing the stability of protrusions. *iScience*. 2024;27(4):109440.

doi: 10.1016/j.isci.2024.109440

51. Kim K, Lee S, Kang H, *et al*. Dual specificity kinase DYRK3 promotes aggressiveness of glioblastoma by altering mitochondrial morphology and function. *Int J Mol Sci*. 2021;22(6):2982.

doi: 10.3390/ijms22062982

52. Sun J, Zhang Y, Li A, Yu H. Dual-specificity tyrosine phosphorylation-regulated kinase 3 expression and its correlation with prognosis and growth of serous ovarian cancer: correlation of DYRK3 with ovarian cancer survival. *Int J Genom*. 2024;2024:6683202.

doi: 10.1155/2024/6683202

53. Akbarzadeh M, Vahedian V, Hamid Abudulmohesen Z, *et al*. The evaluation of melatonin and EGF interaction on breast cancer metastasis. *Horm Mol Biol Clin Investig*. 2024;45(3):119-130.

doi: 10.1515/hmbci-2023-0082

54. Niu X, Chen J, Ma N, *et al*. Nuclear-targeted EGF receptor enhances proliferation and migration of human anaplastic thyroid cancer cells. *Endokrynol Pol*. 2022;73(5):803-811.

doi: 10.5603/EP.a2022.0048

55. Qin H, Liu J, Yu M, *et al*. FUT7 promotes the malignant transformation of follicular thyroid carcinoma through α1,3-fucosylation of EGF receptor. *Exp Cell Res*. 2020;393(2):112095.

doi: 10.1016/j.yexcr.2020.112095

56. He X, Deng B, Zhang C, *et al*. HSPA1A inhibits pyroptosis and neuroinflammation after spinal cord injury via DUSP1 inhibition of the MAPK signaling pathway. *Mol Med*. 2025;31(1):53.

doi: 10.1186/s10020-025-01086-9

57. Lettini G, Pietrafesa M, Lepore S, *et al*. Heat shock proteins in thyroid malignancies: potential therapeutic targets for poorly-differentiated and anaplastic tumours? *Mol Cell Endocrinol*. 2020;502:110676.

doi: 10.1016/j.mce.2019.110676

58. Scieglinska D, Piglowski W, Chekan M, Mazurek A, Krawczyk Z. Differential expression of HSPA1 and HSPA2 proteins in human tissues; tissue microarray-based immunohistochemical study. *Histochem Cell Biol*. 2011;135(4):337-350.

doi: 10.1007/s00418-011-0791-5

59. Sarkar T, Dhar S, Chakraborty D, *et al*. FOXP3/HAT1 axis controls Treg infiltration in the tumor microenvironment by inducing CCR4 expression in breast cancer. *Front Immunol*. 2022;13:740588.

doi: 10.3389/fimmu.2022.740588

60. Gu X, Chen B, Zhang S, Zhai X, Hu Y, Ye H. The expression of CCL17 and potential prognostic value on tumor immunity in thyroid carcinoma based on bioinformatics analysis. *Sci Rep*. 2024;14(1):31580.

doi: 10.1038/s41598-024-75750-1

61. Taniuchi K, Furihata M, Naganuma S, Saibara T. ARHGEF4 predicts poor prognosis and promotes cell invasion by influencing ERK1/2 and GSK-3α/β signaling in pancreatic cancer. *Int J Oncol*. 2018;53(5):2224-2240.

doi: 10.3892/ijo.2018.4549

62. Inoue H, Kanda T, Hayashi G, *et al*. A MAP1B-cortactin-Tks5 axis regulates TNBC invasion and tumorigenesis. *J Cell Biol*. 2024;223(3):e202303102.

doi: 10.1083/jcb.202303102

63. Imai T, Baba M, Nishimura M, Kakizaki M, Takagi S, Yoshie O. The T cell-directed CC chemokine TARC is a highly specific biological ligand for CC chemokine receptor 4. *J Biol Chem*. 1997;272(23):15036-15042.

doi: 10.1074/jbc.272.23.15036

64. Zhang M, Zou B, Li Q, Zhao Y, He Y. Constructing a chemokine-based model and identifying CCL17 as a core biomarker associated with immune infiltrates in thyroid cancer. *Transl Cancer Res*. 2025;14(9):5720-5744.

doi: 10.21037/tcr-2024-2654

65. Baitsch D, Bock HH, Engel T, *et al*. Apolipoprotein E induces antiinflammatory phenotype in macrophages. *Arterioscler Thromb Vasc Biol*. 2011;31(5):1160-1168.

doi: 10.1161/atvbaha.111.222745

66. Ogbodo E, Michelangeli F, Williams JHH. Exogenous heat shock proteins HSPA1A and HSPB1 regulate TNF-α, IL-1β and IL-10 secretion from monocytic cells. *FEBS Open Bio*. 2023;13(10):1922-1940.

doi: 10.1002/2211-5463.13695

67. Šelemetjev S, Bartolome A, Išić Denčić T, *et al*. Overexpression of epidermal growth factor receptor and its downstream effector, focal adhesion kinase, correlates with papillary thyroid carcinoma progression. *Int J Exp Pathol*. 2018;99(2):87-94.

doi: 10.1111/iep.12268

68. Takayama K, Ichiki M, Tokunaga S, *et al*. Randomized phase II study of weekly paclitaxel plus carboplatin versus biweekly paclitaxel plus carboplatin for patients with previously untreated advanced non-small cell lung cancer. *Oncologist*. 2019;24(11):1420-e1010.

doi: 10.1634/theoncologist.2019-0513

69. Takaya H, Nakai H, Murakami K, *et al*. Efficacy of weekly administration of paclitaxel and carboplatin for advanced ovarian cancer patients with poor performance status. *Int J Clin Oncol*. 2018;23(4):698-706.

doi: 10.1007/s10147-018-1264-9

70. Iwaki S, Kawakita D, Sawabe M, *et al*. Long-term efficacy of weekly paclitaxel therapy in unresectable primary squamous cell carcinoma of the thyroid. *Auris Nasus Larynx*. 2022;49(6):1083-1087.

doi: 10.1016/j.anl.2021.06.005